ADVANCED ELECTRONIC MATERIALS
www.advelectronicmat.de

Electrochemical Mechanics of Metal Thin Films: Charge-Induced Reversible Surface Stress for Actuation

Chuan Cheng, Patrick S. Grant, and Lukas Lührs*

The intrinsic charge-induced surface stress of Ni thin films during electrochemical reactions with an alkaline electrolyte is measured in situ. Surface stresses induced by H absorption/desorption, α-Ni(OH)$_2$ formation, capacitive double-layer charging, the α- to β-Ni(OH)$_2$ transformation, and β-Ni(OH)$_2$/β-NiOOH redox reactions are identified, and each provided additive contributions to the overall stress state. Surface stresses are magnified in high-surface-area nanoporous Ni because local stress-relaxation mechanisms are restricted when compared to a smooth Ni film. Ni film reversible tensile/compressive surface stresses correlate with anodic/cathodic potential scanning but with an opposite trend to that of a less reactive Au film. Surface stresses in the Ni films are up to 40 times that of Au films and suggest the possibility of using controlled surface-stress generation for electrochemical actuation.

The measurement of electrode surface stresses induced by electrochemical processes at an electrode/electrolyte interface provides a method to probe the underlining atomistic processes and chemical changes related to charge transfer.[1] These surface stresses are also of critical importance in the thermodynamics of electrode surfaces, including aspects of surface reconstruction, self-organization, electrocatalysis, and electrochemical actuation.[2] Investigations of electrode surface stress have mainly concerned noble metals where the surface stress is induced by sub-monolayer adsorbates in an electrochemical double layer, which changes the electron distribution of surface atoms and induces reversible elastic strain, with reversible surface stresses of the order of 1 N m^{-1}, for Au, Pt, Pd, Ag, and Ir noble metals in various electrolytes.[3]

Dr. C. Cheng, L. Lührs
Institute of Materials Physics and Technology
Hamburg University of Technology
21073 Hamburg, Germany
E-mail: Chuan.Cheng@warwick.ac.uk
Dr. C. Cheng, Prof. P. S. Grant
Department of Materials
University of Oxford
Oxford OX1 3PH, United Kingdom
Dr. C. Cheng
Warwick Manufacturing Group (WMG)
University of Warwick
Coventry CV4 7AL, United Kingdom
The ORCID identification number(s) for the author(s) of this article can be found under https://doi.org/10.1002/aelm.201900364.

DOI: 10.1002/aelm.201900364

Investigation of surfaces stress in more chemically active transition metals, such as Ni, Co, Mn, are by comparison rare. The electrode/electrolyte interfaces of transition metals are intrinsically different from noble metals because more complex, higher strain and stress pseudocapacitive reactions may take place, rather than simply sub-monolayer adsorbates.[4] For example, the charge-induced reversible strain measured in nanoporous Ni has been shown to be one order of magnitude larger than that of a similar nanoporous noble metal[5] with resulting surface distortions observable with the naked eye.[6] As we show below, in situ measurement of surface stress, even in complex cases, can resolve sufficient detail that specific reactions can be deconvoluted and isolated. We also demonstrate that these surface stress effects can be enhanced by a nanoporous surface morphology, which may provide an opportunity for the development of electrochemical microactuators based on low cost transition metals.[3b,7]

The charge-induced surface stress of a Ni film sputtered onto a Si wafer substrate was measured in situ by a multiple-beam optical stress sensor (MOSS) system combined with an electrochemical cell (**Figure 1**a).[8] During electrochemical reactions, if the interatomic distance of the film tends to contract but is restricted by the substrate, a tensile stress is developed in the film and the system is bowed into a concave shape on the Ni side (Figure 1b). If the film tends to expand but is again restricted by the substrate, a compressive stress is developed in the film and the system bows on the convex side (Figure 1c).

From Stoney's equation,[9] the surface stress of the Ni film is given as

$$\Delta f = \langle \Delta\sigma \rangle h_f = \frac{Y_s h_s^2 \cos\alpha}{12(1-\nu_s) L n} \frac{\Delta d}{d_0} \quad (1)$$

where $\langle \Delta\sigma \rangle$ is the change of mean biaxial stress of the film; h_f (=18 nm) and h_s (=200 µm) are the thickness of the film and the substrate, respectively; Δd is the change of the reflected beam spacing with respect to the initial beam spacing d_0; $\Delta d/d_0$ is the ratio measured by the MOSS system; Y_s (=130.2 GPa) and ν_s (=0.279) are Young's modulus and Poisson's ratio of the Si substrate, respectively; n (=1.33) is the refractive index of the electrolyte; α (=3°) is the incident beam angle; and L (=105 cm) is the distance between the cantilever and the CCD camera. In Equation (1), Δf with units of N m^{-1}, is typically referred to as the "surface stress" in the literature but is more strictly the mean film stress × film thickness product.[10] Further details are provided in the Supporting Information.

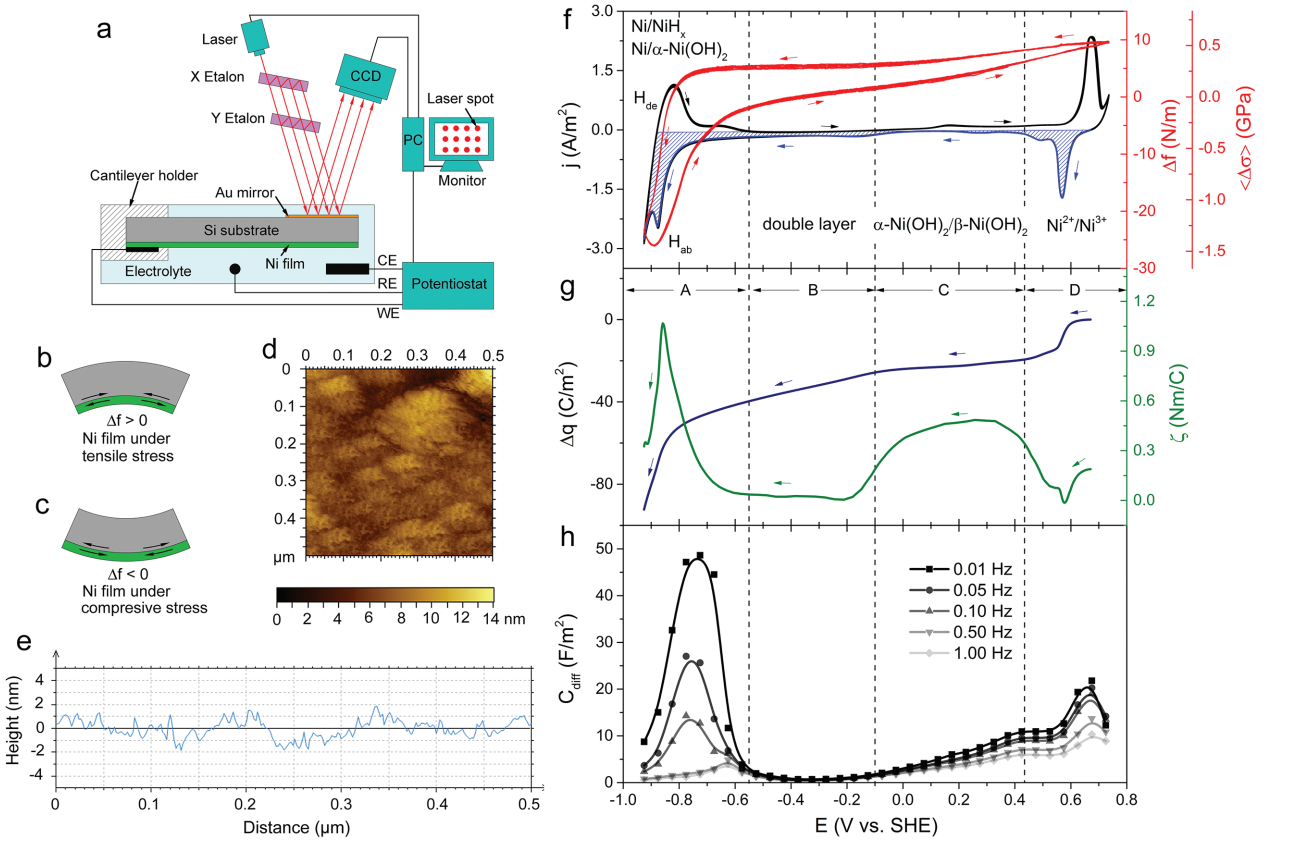

Figure 1. a) Illustration of the experimental set-up for the in situ measurement of surface stress of a Ni thin film. Geometric changes of the cantilever when the Ni film is under b) tensile and c) compressive stresses. d) Scanning tunneling microscope image of the sputtered Ni film and e) the associated surface roughness profile. f) Cyclic voltammetry of a Ni film at 5 mV s^{-1} in 1 M NaOH (left axis), induced surface stress change Δf, and mean biaxial stress change $\langle\Delta\sigma\rangle$ (right axis). g) Charge density integrated for a reduction process (blue region in f)), and the corresponding surface stress–charge coefficient ς (right axis) against potential E. h) Differential capacitance C_{diff} against potential at frequencies from 0.01 to 1.00 Hz.

Scanning tunneling microscopy (STM) investigations of the as-sputtered Ni film showed a comparatively smooth surface with a mean height variation of ± 2 nm (Figures 1d,e) and electrode surface area of 3.2 cm^2 used in subsequent current areal density determination. The film thickness was approximately 18 nm measured by a spectroscopic ellipsometer (Figure S1, Supporting Information).

Over six successive cyclic voltammetry (CV) cycles in Figure 1f, both current and induced Δf were highly reversible and four different electrochemical processes could be distinguished,[11] which provided additive contributions to the overall surface stress. During negative potential scanning starting from –0.550 to –0.925 V in region A of Figure 1f, H absorption[12] led to a sharp drop in surface stress from 5.4 N m^{-1} to –23.3 N m^{-1} and contributed ≈80% of the overall surface stress of 35.9 N m^{-1}. The right-hand side of Figure 1f also shows the mean biaxial stress of the film obtained from $\langle\Delta\sigma\rangle = \Delta f/h_f$ reached an overall amplitude of 2.0 GPa. The surface stress–charge coupling coefficient ($\varsigma = df/dq$, where q is the charge density), on the right-hand side of Figure 1g, reached a maximum of $\varsigma = 1.07$ Nm C^{-1} at –0.858 V during H adsorption, and similar to H absorption in other metals, for example, Pd ($\varsigma = 1.4 \pm 0.2$ Nm C^{-1}),[13] Pd ($\varsigma = 1.2$ Nm C^{-1}),[14] and Pt ($\varsigma = 1.5$ Nm C^{-1}).[15] Absorbed H typically occupies octahedral lattice sites to form β-NiH, which has a lattice constant 3.731 Å and 5.7% larger than that of Ni.[16] At a scan rate of 1 mV s^{-1}, the atomic ratio of H/Ni can reach ≈0.5 and induce a compressive biaxial stress ≈2.6 GPa in the Ni film (see Supporting Information).

As the scanning was switched to the positive direction from –0.925 V, the surface stress in Figure 1f was partially relieved by H desorption at –0.550 V because a Ni → α-$Ni(OH)_2$ reaction took place at the same time,[11] as indicated by the corresponding current plateau from –0.716 to –0.614 V. α-$Ni(OH)_2$ formation induced surface expansion and partially compensated for the H desorption induced contraction. Differential capacitance ($C_{diff} = Y''/\omega$, where Y'' is the imaginary part of the admittance measured by electrochemical impedance spectroscopy and ω is angular frequency)[17] peaked at –0.725 V corresponding to the α-$Ni(OH)_2$ formation and H desorption (Figure 1h). The strong frequency dependence of C_{diff} in Figure 1h suggested that C_{diff} was made up of both double layer capacitance and absorption capacitance.[17]

The flat current in region B was attributed to the capacitive double-layer behaviour, where surface stress increased linearly with potential (Figure 1f).[3b] C_{diff} was at a minimum of 40 μF cm^{-2}, which was consistent with the double layer capacitance of oxidized Ni (40–60 μF cm^{-2}).[18] In region C, an anodic current peak at 0.165 V corresponded to the α-$Ni(OH)_2$

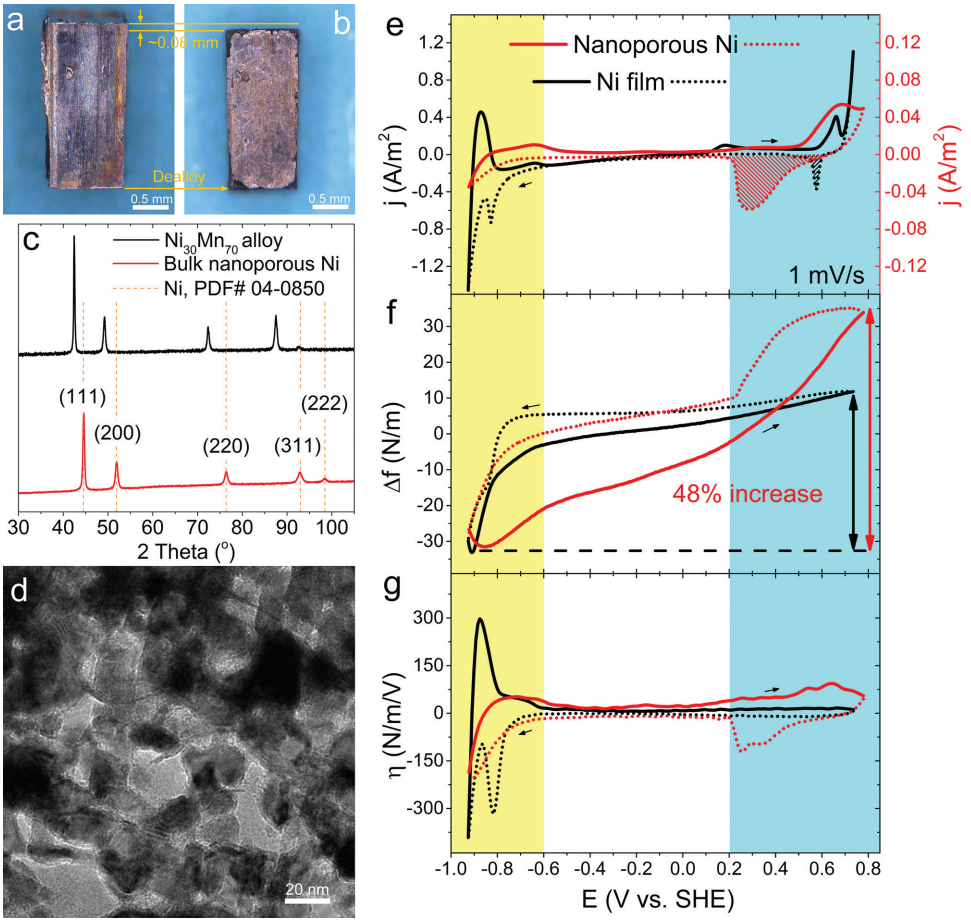

Figure 2. Photograph of a) $Ni_{30}Mn_{70}$ alloy precursor ingot and b) the corresponding dealloyed nanoporous Ni; c) XRD pattern of $Ni_{30}Mn_{70}$ and nanoporous Ni compared with a reference Ni pattern (PDF# 04-0850). d) TEM image of the dealloyed nanoporous Ni. e) cyclic voltammetry of a Ni film (black) and nanoporous Ni (red) at 1 mV s^{-1} in 1 M NaOH electrolyte; f) Charge-induced surface stress of the Ni film was measured by the MOSS system and Equation (1). The nanoporous Ni surface stress determined from the dilatometry strain measurement and Equation (3). g) Derivative of surface stress with respect to potential, in which the derivative of the cathodic scan was multiplied by −1 (dotted curve) to clearly separate the forward and backward scan data.

to β-$Ni(OH)_2$ transformation and was accompanied by lattice shrinkage and thus an increase in surface stress.[19] In region D, an oxidation peak at 0.672 V and a reduction peak at 0.568 V were attributed to the redox reaction β-$Ni(OH)_2 \leftrightarrow \beta$-NiOOH. The forward reaction leads to a lattice shrinkage,[20] again, with a corresponding increase in surface stress.

For comparison, we synthesized 3D millimeter-sized nanoporous Ni samples by dealloying of Mn from a single phase $Ni_{30}Mn_{70}$ solid solution.[5a] **Figures 2**a and 2b show photos of the $Ni_{30}Mn_{70}$ precursor ingot and the corresponding dealloyed nanoporous Ni, respectively. The X-ray diffraction (XRD) pattern of the dealloyed sample confirmed fcc Ni (Figure 2c), while the transmission electron microscopy (TEM) image in Figure 2d confirmed a nanoporous structure with Ni ligament sizes of 13 ± 3 nm between pores.

The electrochemically active surface area of the nanoporous Ni was determined using the behaviour of the much smoother Ni film as follows. First, the charge transferred during the reduction of β-NiOOH → β-$Ni(OH)_2$ was obtained by integrating the CV of the Ni film in the region indicated by the slashed lines in Figure 2e. Then, by assuming that the same charge was transferred per unit area for nanoporous Ni and film Ni at 1 mV s^{-1}, the electrochemically active surface area α_m of nanoporous Ni could be estimated as 9.2 m^2 g^{-1}.

Because the dealloyed Ni was bulk rather than a film, charge-induced dimensional change during CV at the same scan rate as applied to the films was measured instead by dilatometry. The provided a macroscopic strain $\varepsilon = \Delta l/l_0$, where l_0 is the original length of the sample and Δl is the length change, that is, the MOSS system was used for thin film Ni and dilatometry was used for bulk nanoporous Ni.

Dilatometry strain $\varepsilon = \Delta l/l_0$ was then converted to an equivalent surface stress Δf using the capillary equation derived by Weissmüller and Cahn:[21]

$$3V_s \langle \Delta P \rangle_V = 2A \langle \Delta f \rangle_A \quad (2)$$

where A is the total wetted surface area, V_s is the total volume of solid, P is the volumetric mean of the pressure, f denotes surface stress, and the $\langle\rangle$ brackets denote their respective averages and assuming a linear elastic response, $\Delta P = -K\Delta V_s/V_s$, where K (=180 GPa) is the bulk modulus of the solid Ni. The

volume change of the solid ΔV was scaled with the macroscopic length change of nanoporous structure by $\Delta V_s/V_s = 3\Delta l/l_0$. Substituting these relations into Equation (2), we obtain the surface stress–strain relationship for the nanoporous Ni:[22]

$$\Delta f = -\frac{9K}{2\rho\alpha_m}\varepsilon \tag{3}$$

where α_m (=A/m) is the specific surface area of the nanoporous Ni, m is the solid mass, and ρ is the density of solid Ni.

The current peaks for nanoporous Ni were comparatively broad due to relatively sluggish ion transport within the tortuous nanoporous structure (Figure 2e) compared with the film Ni; accordingly, the surface stress in nanoporous Ni had a larger positive/negative scan hysteresis (Figure 2f). The magnitude of charge-induced surface stress in nanoporous Ni (66.6 N m^{-1}) was 48% larger than that of film Ni (44.9 N m^{-1}), indicating an amplification of surface stress.

In Figure 2e, the significant differences between the nanoporous Ni and film Ni the CV curves relate to the electrode morphology—nanoporous or smooth. The nanoporous electrode has a high tortuosity and surface area and its effect on the effective ion diffusion coefficient D_{eff} can be estimated[23] from $D_{eff} = D/\tau^2$, where D is the diffusion coefficient in the bulk electrolyte and τ is the electrode tortuosity. Evidently, the effective ion diffusion coefficient for the nanoporous electrode must be lower than that of the smooth electrode. This reduced ion diffusion coefficient then decreased the peak current of CV curves and increased the peak width, as previously described by Equations (6.4.6) and (6.4.7) in ref. [24]. In addition, the more sluggish ion diffusion within the nanoporous Ni may restrict the H lattice absorption compared with the Ni film at the same scan rate, which had more obvious H absorption /desorption peaks at the negative potential end.

During the β-Ni(OH)$_2$ → β-NiOOH reaction (>0.2 V), surface stress in the nanoporous Ni increased sharply to 34.7 N m^{-1} and contributed 52% of the overall stress, which was more than three times that of film Ni (16%). The surface stress–voltage coupling coefficient was defined as $\eta = df/dE$ and is plotted in Figure 2g to show a pair of strong η peaks corresponding to the redox reactions for nanoporous Ni. η was larger for the nanoporous Ni because its highly curved, torturous geometry restricted local strain relaxation whereas strain was more readily relaxed in the smooth Ni film.

In addition, the scan rate of the CV will affect the strain and stress amplitude of Ni-based electrochemical actuators, which has been reported in our pervious publications, such as Figures 2e and 3a in ref. [5a] and Figure 3b in ref. [6a]. Similar tendencies have been reported by others, such as Figure 2g in ref. [5b]. These papers showed that the strain amplitude decreased quickly with increasing scan rates. However, the signs of the strain did not change, only the amplitude. The origin of this scan rate dependence is because the actuation of the Ni-based material arises from both pseudocapacitive charging and double-layer capacitive charging. The former process has faradic reactions that store more charge, and contribute most of the actuation strain/stress at low CV scan rates. However, the pseudocapacitive process becomes restricted by mass-transport with increasing scan rate and its relative contribution to actuation quickly diminishes. In the contrast, the charge accumulated in the double-layer is a capacitive process with a time constant below a millisecond,[25] and is consequently much less affected by the CV scan rates.

As Au has been used widely as a model material for charge induced stress/strain investigations,[26] the intrinsic charge-stress coupling of Ni film was compared with a similar Au film (**Figure 3**). The current densities produced by the Au film were much smaller than Ni in both the electrochemical stability potential region (Figure 3b) and the redox region (Figure 3f), which reflected the lower capacitance of Au. As a result, surface stress for Ni was approximately 40 times and 7 times that of Au in the corresponding surface stress plots in Figures 3c and 3g, respectively. These differences were reproducible during repeated cycles, as shown in Figure 3d,h.

There were no H absorption/desorption current peaks for Au contributing to strain (Figure 3b, red). In contrast, H absorption/desorption for Ni contributed approximately 80% of the resulting surface stress (Figure 3c, black). Even when surface processes only were considered, Au had a much smaller surface stress response than Ni (Figure 3g). The CV response of the Au film in Figure 3f can be separated into three regions[27]: i) a capacitive double layer region (<0.1 V); ii) a non-oxide region (0.1–0.45 V), and iii) an oxide-region (>0.45 V). The non-oxide region was attributed to the reversible formation of electrosorbed OH- species,[28] with a charge transfer of 2.39 C m^{-2} obtained from CV, which corresponded to a monolayer of adsorbed OH- species on (111) plane (theoretically, 2.23 C m^{-2}), consistent with reports that sputtered Au films on (001)-oriented Si wafers typically have a (111)-oriented surface.[8] With potential increasing to the oxide-region, a broad anodic peak was associated with oxidation of Au(OH)$_{ad}$ toward Au(OH)$_3$,[29] with a total charge transfer of 7.58 C m^{-2} that corresponded to the production of Au(OH)$_{3.4}$. However, considering possible roughness of the Au film, which was neglected in the charge density evaluation, the reaction product may be close to a monolayer of Au(OH)$_3$ formation (>0.45 V).

In the case of the Ni film, for hexagonal structured β-Ni(OH)$_2$ sheets with a Ni–Ni interatomic distance of 3.13 Å,[18] the transferred charge for a monolayer of redox reaction was estimated at 1.89 C m^{-2}. However, there was a transfer charge of 16.88 C m^{-2} in the redox region here, approximating to nine layers of β-Ni(OH)$_2$. By assuming (001) oriented β-Ni(OH)$_2$ at the Ni surface, the thickness of the oxide passive layer was approximately 4.1 nm, which agrees reasonably well with prior X-ray photoelectron spectroscopy measurements.[30] Therefore, a monolayer of Au was oxidized while nine layers of β-Ni(OH)$_2$ were oxidized in the same potential region of Figure 3f, which led to the seven times measured difference in charge-induced surface stress in Figure 3g.

In terms of the surface stress–voltage coupling coefficient $\eta = df/dE$, Figure 3d,h show that Δf for Ni was in-phase with potential ($df/dE > 0$) while Δf for Au was out-of-phase with potential ($df/dE < 0$). From Figure 3g, a linear best-fit of the surface stress to potential gave η = 5.36 N m^{-1} V^{-1} for the Ni film and η = −0.66 N m^{-1} V^{-1} for the Au film. Thus, during positive scanning, the Ni film contracted whereas Au film expanded, as illustrated in Figure 3a,e. The difference in signs of η originated from the nature of the metal surface, that is,

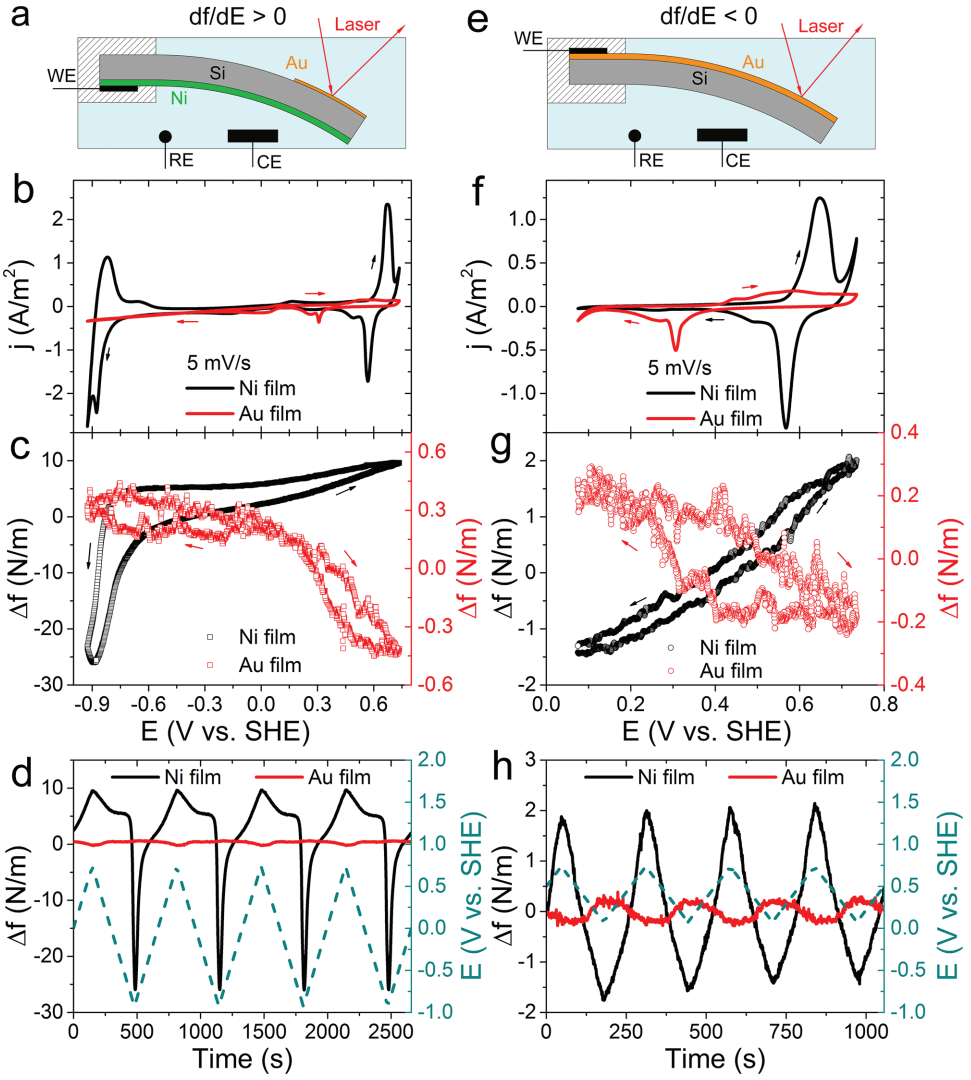

Figure 3. Comparison of the charge-induced surface stresses in Ni and Au thin films during cyclic voltammetry. a,e) Illustration of the cantilever bending during positive potential scanning with Ni and Au thin films as working electrodes, respectively. Cyclic voltammetry of Ni and Au thin films at 5 mV s^{-1} in 1 M NaOH electrolyte within b) [–0.925, 0.735] V versus SHE; and f) [0.075, 0.735] V versus SHE. c,g) Surface stress against potential corresponding to (b) and (f), respectively. d,h) Surface stress (left) and potential (right) against time for cyclic scanning of the Ni and Au thin films.

whether it was covered with oxide ("+" sign) or a "clean" metal surface ("–" sign). At the onset of the oxidation reaction for the redox pair β-$Ni(OH)_2$/β-NiOOH, β-$Ni(OH)_2$ was already present on the Ni surface while Au was not yet oxidized. Here, "clean" metal surface means a surface without (anodic) oxide coverage. Before charging of a clean Au surface, the bonding strength between surface atoms is stronger compared with the bulk due to the redistribution of surface electrons toward in-plane and inner bonds, as a result, the equilibrium interatomic distance of surface atoms is reduced compared with the bulk atoms (surface contraction).[31] Upon positive charging, the excess positive charge reduces surface electron density, and the interatomic distance is increased, which results in localized surface expansion. This actuation mechanism is different from the case of Ni with a surface oxide. The surface stress of Ni is mainly attributed to pseudocapacitive processes with reactants consumption and products formation on the surface (leading to lattice mismatch or lattice volume change) rather than capacitive charge accumulation or release, as explained for Figure 1f.

Figure 4a shows the highly reversible electrochemical actuation of a Ni film during cyclic potential scanning at 1 mV s^{-1} over 15 h. Surface stress contributions from different potential regions could again be easily separated and reproduced in successive cycles. Figure 4b demonstrates that as the potential applied to the Ni film jumped step-wise, the induced strain in nanoporous Ni stabilized after approximately 2 min. This actuation stability is critical for actuator applications that require fixed strain without drift overtime and typically suffered by polymer-based low-voltage actuators such as ionic electroactive polymers,[32] or by nanoporous noble metal-based actuators due to ligament coarsening.[26a]

In summary, the charge-induced surface stress of Ni thin films due to electrochemical processes in an alkaline electrolyte was measured in situ by a MOSS system combined with

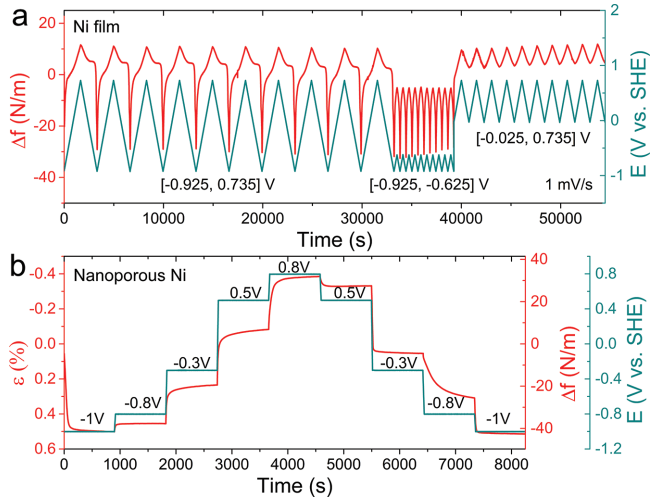

Figure 4. a) The variation of surface stress with time for a Ni film under cyclic potential scanning for different potential windows at 1 mV s^{-1} in 1 M NaOH electrolyte. b) The variation of strain in nanoporous Ni (left) as a function of time and the corresponding surface stress (right) at different potential steps. Please note that the red curve plots both strain and stress, which are linearly related by Equation (3), with the resulting different scales and units given on the left- and right-hand side vertical axes, respectively.

an electrochemical cell. A non-linear, positive-signed surface stress–charge coefficient over a wide potential window comprised the additive effect of different surface stress generation mechanisms. Compared with the Ni film, bulk nanoporous Ni had higher surface stresses due to the highly curved tortuous geometry of the electrolyte/Ni interface that restricted local stress relaxation. Compared with Au thin films measured under the same conditions, the induced surface stresses in Ni film were ≈40 times of Au film within the accessible potential region, and ≈7 times of Au film within the redox region. These significant differences highlighted the advantage of Ni over noble metals for large surface stress generation for possible electrochemical actuation applications.

Supporting Information

Supporting Information is available from the Wiley Online Library or from the author.

Acknowledgements

C.C. thanks the Alexander von Humboldt Foundation, Germany, for a research fellowship. This work received the financial support of the DFG via SFB "M3" subproject B2 and U.K. Engineering and Physical Science Research Council grant EP/P005411/1 (SELFIES). The authors thank Jörg Weissmüller for discussion and comments, Jürgen Markmann for assistance with spectroscopic ellipsometer, Shan Shi for assistance with magnetron sputtering, and Anastasia Straßer for assistance with STM.

Open access funding enabled and organized by Projekt DEAL.

Conflict of Interest

The authors declare no conflict of interest.

Keywords

charge-induced surface stress, electrocapillaries, electrochemical actuators, metal thin films, nanoporous metals

Received: April 10, 2019
Revised: October 25, 2019
Published online: November 18, 2019

[1] a) W. Haiss, *Rep. Prog. Phys.* **2001**, *64*, 591; b) R. C. Cammarata, *Prog. Surf. Sci.* **1994**, *46*, 1; c) R. C. Cammarata, K. Sieradzki, *Annu. Rev. Mater. Sci.* **1994**, *24*, 215.
[2] a) H. Ibach, *Surf. Sci. Rep.* **1997**, *29*, 195; b) P. Müller, A. Saúl, *Surf. Sci. Rep.* **2004**, *54*, 157; c) J. Weissmüller, K. Sieradzki, *MRS Bulletin.* **2018**, *43*, 14.
[3] a) P. J. Feibelman, *Phys. Rev. B* **1997**, *56*, 2175; b) J. Weissmüller, R. N. Viswanath, D. Kramer, P. Zimmer, R. Würschum, H. Gleiter, *Science* **2003**, *300*, 312; c) V. Fiorentini, M. Methfessel, M. Scheffler, *Phys. Rev. Lett.* **1993**, *71*, 1051; d) Q. B. Deng, J. Weissmüller, *Langmuir* **2014**, *30*, 10522.
[4] C. Cheng, A. H. W. Ngan, *ACS Nano* **2015**, *9*, 3984.
[5] a) C. Cheng, L. Lührs, T. Krekeler, R. Ritter, J. Weissmüller, *Nano Lett.* **2017**, *17*, 4774; b) Q. Bai, Y. Wang, J. Zhang, Y. Ding, Z. Peng, Z. Zhang, *J. Mater. Chem. C* **2016**, *4*, 45.
[6] a) C. Cheng, J. Weissmüller, A. H. W. Ngan, *Adv. Mater.* **2016**, *28*, 5315; b) D. Kramer, R. N. Viswanath, J. Weissmüller, *Nano Lett.* **2004**, *4*, 793.
[7] K. W. Kwan, S. J. Li, N. Y. Hau, W.-D. Li, S. P. Feng, A. H. W. Ngan, *Sci. Rob.* **2018**, *3*, eaat4051.
[8] M. Smetanin, R. N. Viswanath, D. Kramer, D. Beckmann, T. Koch, L. A. Kibler, D. M. Kolb, J. Weissmüller, *Langmuir* **2008**, *24*, 8561.
[9] a) G. G. Stoney, *Proc. R. Soc. A* **1909**, *82*, 172; b) Q. V. Overmeere, J. F. Vanhumbeeck, J. Proost, *Rev. Sci. Instrum.* **2010**, *81*, 045106.
[10] J. A. Floro, E. Chason, S. R. Lee, R. D. Twesten, R. Q. Hwang, L. B. Freund, *J. Electron. Mater.* **1997**, *26*, 969.
[11] D. S. Hall, D. J. Lockwood, C. Bock, B. R. MacDougall, *Proc. R. Soc. A* **2015**, *471*, 20140792.
[12] S. A. S. Machado, L. A. Avaca, *Electrochim. Acta* **1994**, *39*, 1385.
[13] L. A. Kibler, A. M. El-Aziz, R. Hoyer, D. M. Kolb, *Angew. Chem., Int. Ed.* **2005**, *44*, 2080.
[14] R. N. Viswanath, J. Weissmüller, *Acta Mater.* **2013**, *61*, 6301.
[15] J. Weissmüller, R. N. Viswanath, L. A. Kibler, D. M. Kolb, *Phys. Chem. Chem. Phys.* **2011**, *13*, 2114.
[16] a) B. Predel, in *Phase Equilibria, Crystallographic and Thermodynamic Data of Binary Alloys Ga-Gd—Hf-Zr* (Ed: O. Madelung), Springer, Berlin **1996**, pp. 1–6; b) N. Takano, S. Kaida, *ISIJ Int.* **2012**, *52*, 263.
[17] V. D. Jovic, B. M. Jovic, *J. Electroanal. Chem.* **2003**, *541*, 1.
[18] D. S. Hall, Ph.D. thesis, University of Ottawa **2014**.
[19] R. S. McEwen, *J. Phys. Chem.* **1971**, *75*, 1782.
[20] M. B. J. G. Freitas, *J. Power Sources* **2001**, *93*, 163.
[21] J. Weissmüller, J. W. Cahn, *Acta Mater.* **1997**, *45*, 1899.
[22] J. Weissmüller, H. L. Duan, D. Farkas, *Acta Mater.* **2010**, *58*, 1.
[23] a) J. van Brakel, P. M. Heertjes, *Int. J. Heat Mass Transfer* **1974**, *17*, 1093; b) L. Shen, Z. Chen, *Chem. Eng. Sci.* **2007**, *62*, 3748.
[24] A. J. Bard, L. R. Faulkner, *Electrochemical Methods: Fundamentals and Applications*, John Wiley & Sons, New York **2001**.
[25] J. Lück, A. Latz, *Phys. Chem. Chem. Phys.* **2018**, *20*, 27804.
[26] a) H. J. Jin, J. Weissmüller, *Science* **2011**, *332*, 1179; b) C. Stenner, L. H. Shao, N. Mameka, J. Weissmüller, *Adv. Funct. Mater.* **2016**, *26*,

5174; c) L. Lührs, B. Zandersons, N. Huber, J. Weissmüller, *Nano Lett.* **2017**, *17*, 6258.
[27] H. Angerstein-Kozlowska, B. E. Conway, B. Barnett, J. Mozota, *J. Electroanal. Chem. Interfacial Electrochem.* **1979**, *100*, 417.
[28] R. Cordova O, M. E. Martins, A. J. Arvia, *Electrochim. Acta* **1980**, *25*, 453.
[29] R. Cordova O, M. E. Martins, A. J. Arvia, *J. Electrochem. Soc.* **1979**, *126*, 1172.
[30] H. W. Hoppe, H. H. Strehblow, *Surf. Interface Anal.* **1989**, *14*, 121.
[31] a) F. Weigend, F. Evers, J. Weissmüller, *Small* **2006**, *2*, 1497; b) H. J. Jin, S. Parida, D. Kramer, J. Weissmüller, *Surf. Sci.* **2008**, *602*, 3588.
[32] Y. Bar-Cohen, *Electroactive Polymer (EAP) Actuators as Artificial Muscles: Reality, Potential and Challenges*, 2nd ed., SPIE Press, Bellingham, WA **2004**.